ARTICLE

Double-Resonance Plasmon Substrates for Surface-Enhanced Raman Scattering with Enhancement at Excitation and Stokes Frequencies

Yizhuo Chu, Mohamad G. Banaee, and Kenneth B. Crozier*

School of Engineering and Applied Sciences, Harvard University, 29 Oxford Street, Cambridge, Massachusetts 02138

ABSTRACT We report a surface-enhanced Raman scattering (SERS) substrate with plasmon resonances at both excitation and Stokes frequencies. This multilayer structure combines localized surface plasmons on the nanoparticles with surface plasmon polaritons excited on a gold film. The largest SERS enhancement factor for a gold device is measured to be 7.2×10^7, which is more than 2 orders of magnitude larger than that measured on a gold nanoparticle array on a glass substrate. The largest SERS enhancement for a silver device is measured to be 8.4×10^8.

KEYWORDS: localized surface plasmon · surface plasmon polariton · nanoparticle · surface enhanced Raman scattering · spatial distribution · hybridization

Surface-enhanced Raman scattering (SERS) refers to the phenomenon whereby Raman scattering is significantly enhanced when molecules are adsorbed on metallic nanostructures.[1] SERS is a powerful analytical technique, enabling molecules to be identified from their vibrational spectra at very low concentrations. The huge enhancement mainly arises from two mechanisms: electromagnetic (EM) enhancement and chemical enhancement.[1] The EM mechanism is related to the enhancement in the near field intensity as a result of the excitation of surface plasmons.[2] Chemical mechanism is attributed to electronic coupling between the adsorbed molecules and the metal surface.[3] It is believed that the EM enhancement accounts for the majority of the enhancement factor and the chemical enhancement only contributes a small portion of the enhancement on the order of $10-10^2$.[4]

Noble metallic nanoparticles have been shown to be highly effective as SERS substrates.[5−10] The excitation of localized surface plasmons (LSPs), collective electron oscillations in the nanoparticles, leads to giant enhancement of the local electromagnetic field.[11] The LSP resonance properties of a metal nanoparticle depend on its size, shape, and the permittivity, as well as the dielectric environment.[12] To increase the enhancement of the near field, many studies have optimized the nanoparticle geometry.[13−15] Studies have also been carried out on combining LSPs with other phenomena, such as grating diffraction effects, waveguides, and metal films, to obtain favorable properties.[16−21]

The SERS EM enhancement factor is proportional to the product of the field intensity ($|E^2|$) enhancements at the excitation and Raman scattering frequencies.[1] For an LSP with a single resonance, it has been shown that the maximum SERS enhancement occurs when the LSP resonance is located between the excitation and the Raman scattering frequencies.[5] A large proportion of SERS research has employed substrates that provide a single LSP resonance.

Here, we investigate a double-resonance SERS substrate that has advantages compared to single-resonance SERS structures. Recently, we demonstrated strong coupling between LSPs and surface plasmon polaritons (SPPs) in a structure consisting of a gold disk array, an SiO_2 spacer, and a continuous gold film.[22] In this work, we investigate the use of this structure for SERS, motivated by the increased field enhancement predicted by our previous study,[22] in comparison to nanoparticles on a glass substrate (with no gold film). Our electromagnetic simulations predicted that the intensity enhancement (square of electric field, $|E^2|$) on the surface of a single gold disk separated from a gold film by a spacer layer is 1 order of magnitude higher than that of a gold disk with the same dimensions on a

*Address correspondence to kcrozier@seas.harvard.edu.

Received for review December 14, 2009 and accepted April 15, 2010.

Published online April 29, 2010. 10.1021/nn901826q

glass substrate.[22] This is due to the interaction between the localized surface plasmon on the gold disk and its image excited in the gold film.[22] In addition, the simulations predicted that the intensity enhancement of each disk of an array above a gold film is twice as large as that of a single disk above a gold film.[22] This is due to the fact that, when the array periodicity is appropriately chosen, the strong coupling between the LSP and the SPP enhances the near field intensity.[22] Besides the large near field enhancement, the structure has a double-resonance spectrum, which is another favorable feature for SERS. Different from single-resonance structures, the double-resonance structure, with near-field intensity peaking at two resonance frequencies, presents the opportunity for simultaneous enhancement at both the excitation and the specific Raman Stokes lines.

In this work, we present results on the use of double-resonance plasmon substrates for SERS. SERS spectra of benzenethiol molecules adsorbed on double-resonance substrates with different periods are shown. The SERS enhancement factor (EF) for the double-resonance structure is found to be more than 2 orders of magnitude larger than that of a regular gold nanoparticle array on a glass substrate. We find that the double resonance structure with optimal array period produces considerably higher SERS EF than the structures with nonoptimal periods. In fact, despite the fact that the optimal structure is less dense, that is, has a larger array period, the total SERS signal is found to be larger than those obtained from more densely spaced structures with nonoptimal periods due to the larger EF. The largest SERS enhancement factor for the 1074 cm^{-1} Raman line of the benzenethiol molecule is measured to be 8.4×10^8.

The schematic of the structure is shown in Figure 1a. The gold device consists of a 100 nm thick unpatterned gold film, an SiO_2 spacer and a square gold disk array. The fabrication method is described in ref 22. A scanning electron micrograph (SEM) of the fabricated structure is shown as Figure 1b. The thickness of the SiO_2 spacer is 23 nm and the refractive index of the SiO_2 is 1.44, as measured by ellipsometry. The overall size of the gold disk array is 100×100 μm. The array periods vary from 350 to 780 nm. The gold disks are 40 nm thick, with diameters ranging from 120 to 140 nm. The silver device consists of a 100 nm thick silver film, an SiO_2 spacer deposited by ebeam evaporation, and a square silver disk array. The SiO_2 spacer is 27 nm thick and the refractive index of the SiO_2 spacer is 1.44, as measured by ellipsometry. The silver disks are 40 nm thick, with diameters ranging from 140 to 150 nm. The array period is 780 nm. For the SERS measurements, self-assembled monolayers of benzenethiol molecules are formed on the gold disks. This is performed by immersing the devices in a 3 mM solution of benzenethiol in ethanol for

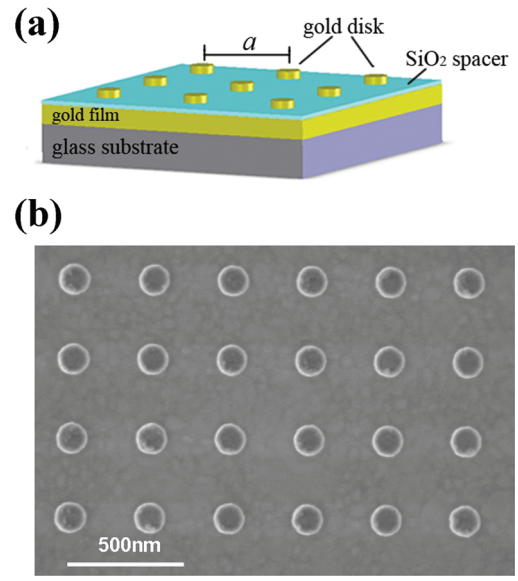

Figure 1. (a) Schematic of gold double resonance structure. (b) Scanning electron micrographs (SEM) of gold disk array on SiO_2 spacer and gold film.

1 h, rinsing with neat ethanol, and then blow drying with nitrogen.

The double resonance structure we investigate here combines LSP and SPP resonances. The LSP resonance frequency is determined by the size and shape of the

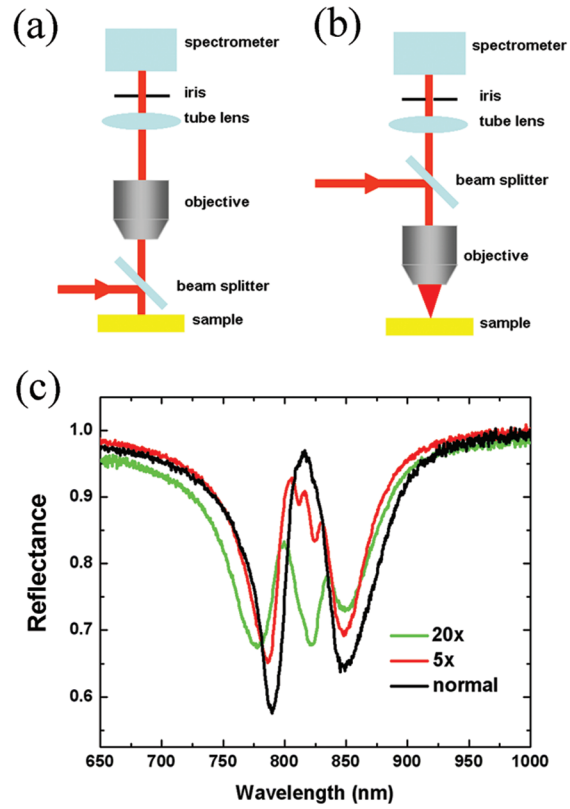

Figure 2. Reflection measurement setups for (a) collimated incidence and (b) focused incidence. (c) Measured reflection spectra of gold disk array on SiO_2 and gold film for collimated and focused incidences (5× or 20× objectives). Gold disks are 130 nm in diameter and are 40 nm thick. Array period is 780 nm.

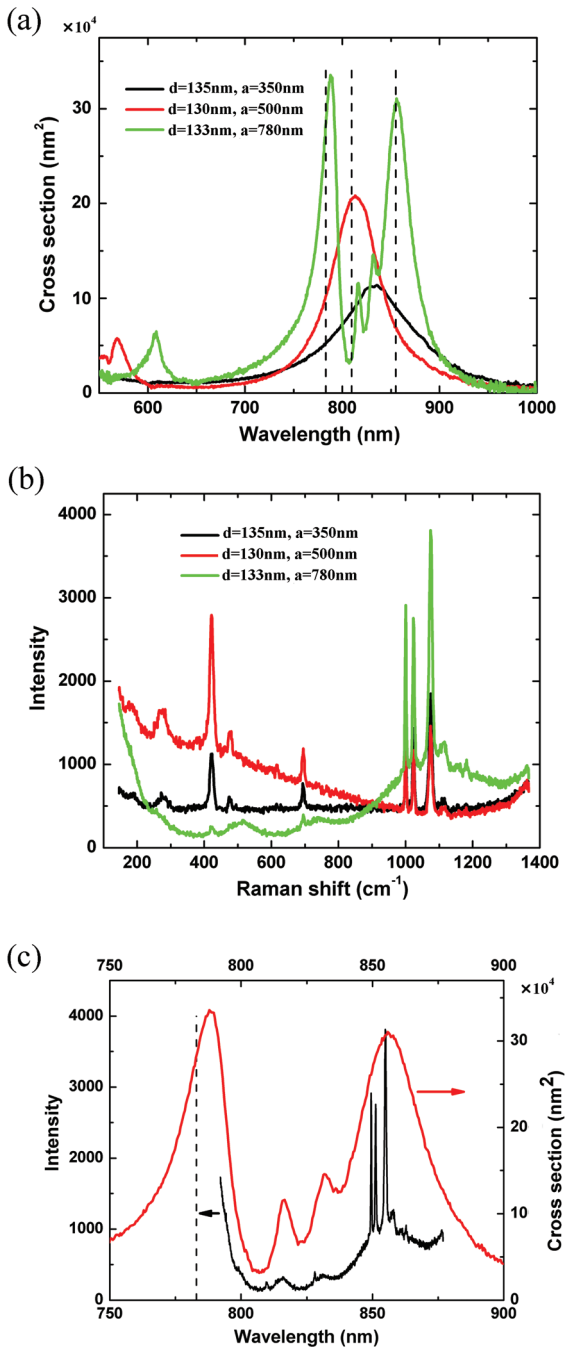

Figure 3. (a) Extinction cross sections for three gold disk arrays on SiO_2 and gold film: black, disk diameter d = 135 nm, array period a = 350 nm; red, disk diameter d = 130 nm, array period a = 500 nm; green, disk diameter d = 133 nm, array period a = 780 nm; dashed lines, wavelengths of the excitation, 420 and 1074 cm^{-1} Raman lines. (b) SERS spectra for three structures. CCD integration time: 30 s. (c) Extinction cross section and SERS spectrum of array with period of 780 nm.

gold disk, as well as the refractive index of the surrounding medium. On the other hand, the SPP resonance frequency is determined by the component of the wavevector parallel to the interface, in addition to the refractive indices of the gold and of the surrounding medium. It is therefore determined by the array period and the angle of incidence of the illumination. We hence expect the illumination and collection configurations to influence the SERS measurements. To investigate this, we measure far field reflection spectra with collimated and focused illumination. The setups are shown in Figure 2a,b. In the collimated incidence case, a collimated white light beam illuminates the structure through a beam splitter, with the reflected light being collected by a 10× objective. In the focused incidence case, the incident light is focused by either a 5× objective (NA = 0.1) or a 20× objective (NA = 0.4), with the reflected light being collected by the same objective. The reflected light is collected into a spectrometer. An iris is used at the image plane of the objective to ensure that only the light reflected by the array is detected. To account for the spectrum of the source (Xe lamp), the transmission spectra of the optical components, and the detector response, reference measurements are made. These consist of spectra measured on a region of the sample away from the gold disk array, that is, consisting of the SiO_2 spacer on gold film. These spectra are recorded under identical conditions as the spectra of the gold disk arrays. The normalized reflection spectra are then found by dividing the gold disk array spectra by the reference spectra. This method therefore takes the reflectance of the gold film and spacer layer to be unity, for simplicity. Normalized reflection spectra of a gold disk array with period of 780 nm on an SiO_2 spacer with an underlying gold film under collimated or focused (5× or 20× objective) illumination are shown as Figure 2c. The gold disks are 130 nm in diameter. For this period and disk diameter, the resonance frequency of the LSP of a single, isolated gold disk above a gold film (with a spacer layer) would be approximately equal to the resonance frequency of the SPP mode, were they uncoupled. In the structure under study, however, the LSP and SPP are strongly coupled, leading to the repulsion of the resonances seen in the spectrum obtained with collimated incidence. In the spectrum collected by the 5× objective with a NA of 0.1, some small features can be seen between the two primary resonances. These small features are due to the spread in the illumination angles. As the spread of the incident angle increases with the use of a larger NA objective (20×, NA = 0.4), the features in the middle become prominent. These additional resonances are believed to be related to the field polarized normal to the sample surface, which excites the vertical particle resonance.[23] It also can be seen that the resonance depth decreases as the NA of the objective increases, implying that the near field enhancement is larger for the smaller spread of incident angles. However, the Raman spectrometer used for the SERS measurements (Renishaw confocal microscope) does not allow collimated illumination, unlike the setup of Figure 2a. As described later, we therefore perform SERS measurements using a 5× objective with a low NA.

To characterize the optical properties of the structures used in the SERS measurements, reflection mea-

surements are made using the setup shown in Figure 2b, equipped with a 5× objective with an NA of 0.1. The adsorption of benzenethiol molecules on the gold disks can result in shifts of the LSP and SPP resonances because it changes the refractive index of the medium surrounding the gold disks. The reflection spectra are therefore taken after the formation of the benzenethiol monolayer. To compare the optical properties of samples with different periodicities, the extinction cross section associated with each gold disk is found. This quantity is calculated from the normalized reflection spectra by the relation $C_{ref} = (1 - R) \times a^2$, where R is the normalized reflectance and a is the period of the array. The disk diameter and the array period are chosen so that plasmon resonances occur at the wavelengths of the excitation and of the 1074 cm^{-1} Raman line of benzenethiol. Figure 3(a) plots the extinction cross sections as a function of wavelength for three structures. For the first structure (black curve), the gold disks have diameters of 135 nm and a period of 350 nm. The resonance at 833 nm corresponds to the LSP of the gold disks. For the second structure (red curve), the gold disks have diameters of 130 nm and a period of 500 nm. The resonance at 813 nm corresponds to the LSP of the disks, and the small resonance at 568 nm corresponds to the $(p,q) = (1,0)$ SPP mode. Here, (p,q) refers to the reciprocal lattice vector of $G = (2\pi/a)\sqrt{p^2 + q^2}$ provided by the lattice, where a is the period. For these two structures, the LSP and SPP are weakly coupled. For the third structure (green curve), the gold disks have diameters of 133 nm and a period of 780 nm. In contrast to the first two structures, the LSP and SPP are strongly coupled, resulting in repulsion of the resonances, as described previously. The peak value of the cross section for the strong coupling case is larger than that of the weak coupling cases, implying that the coupling of LSP and SPP enhances the local field still further. These results are consistent with the simulation predictions.[22]

To investigate the near field properties of the structures, we use the finite-difference time-domain (FDTD) method to calculate the near field spectra and the near field intensity distribution. Using the same method described in ref 22, we first simulate the near field spectra for the structure with array periods of 500 (weak coupling) and 780 nm (strong coupling). The field intensity at the edge of the gold disk at the interface between the gold disk and the SiO_2 spacer is recorded. The gold disk is 133 nm in diameter and 40 nm thick. The SiO_2 spacer is 25 nm thick with refractive index of 1.44. Figure 4a shows the near field spectra. The structure with period of 500 nm (black curve) has a resonance at $\lambda = 827$ nm, which corresponds to the LSP resonance and a small feature at $\lambda = 586$ nm, which corresponds to the (1,0) SPP mode at the interface of the gold film and the SiO_2 spacer. The structure with period of 780 nm (red curve) has double resonances at $\lambda = 794$ and 860 nm

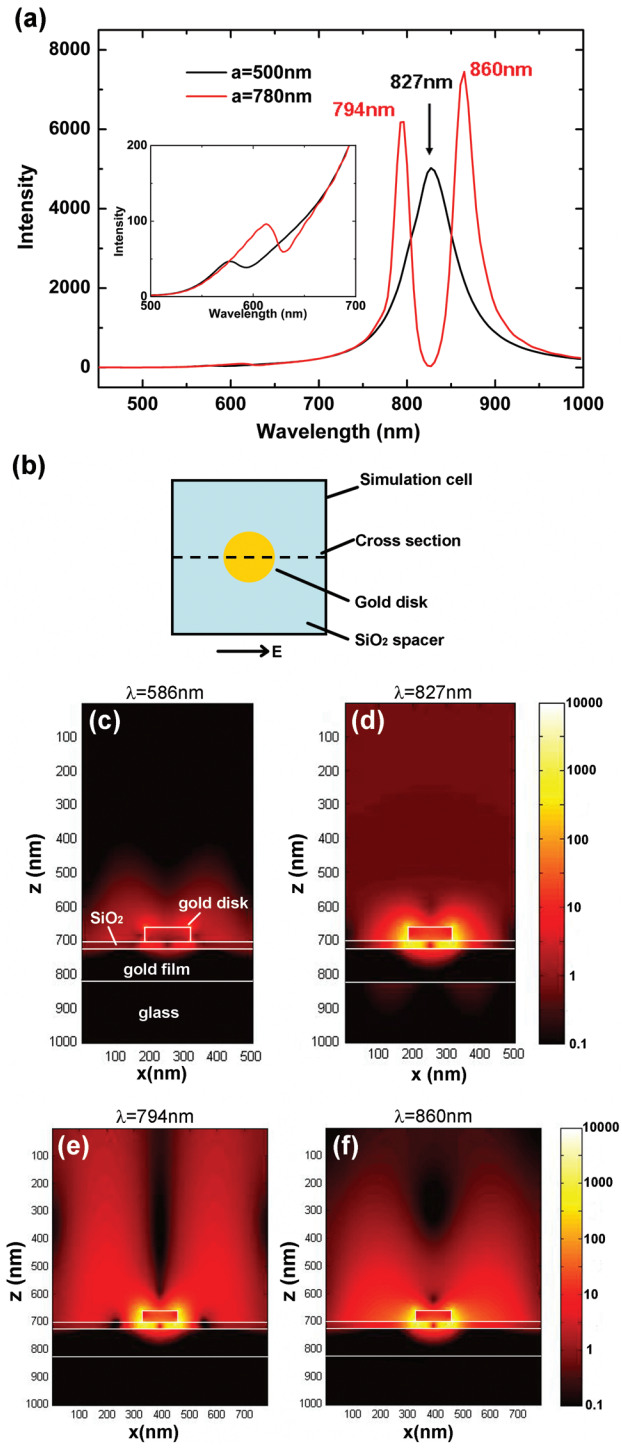

Figure 4. (a) Simulated near field intensity spectra: gold disk diameter, 133 nm; SiO_2 spacer thickness, 25 nm; black, weak coupling case with array period of 500 nm; red, strong coupling case with array period of 780 nm. Inset: expanded view of near field spectra over the range $\lambda = 500$ nm to 700 nm. (b) Top view of the structure in the simulation. (c−f) Intensity ($|E_s|^2$) distributions of scattered field on the cross section perpendicular to substrate for illumination at (c) $\lambda = 586$ nm and at (d) $\lambda = 827$ nm for the 500 nm period array, at (e) $\lambda = 794$ nm and at (f) $\lambda = 860$ nm for the 780 nm period array.

and a small feature at $\lambda = 627$ nm corresponding to the (1,1) SPP mode on the gold film. We calculate the field intensity ($|E|^2$) distribution on the cross sections

perpendicular to the substrate for excitation at λ = 586 and 827 nm for the 500 nm period array and at 794 and 860 nm for the 780 nm period array. The cross section's position is shown in Figure 4b. The interference between the incident field and its reflection from the gold film gives a fringe pattern in the space above the gold film that complicates physical interpretation of the field patterns arising from the LSP and SPP resonances. To mitigate this, we therefore calculate the intensity of the scattered, rather than total, field. Reference calculations are made of structures consisting of an SiO_2 spacer on an unpatterned gold film. The scattered field E_s is then obtained by subtracting the field of the reference calculation from the field calculated for the SERS substrate, that is, with the addition of the gold disks. In this way, the fields arising from the LSP and SPP resonances can be visualized. Figure 4c−f show the scattered field intensity ($|E_s|^2$) distribution at λ = 586 and 827 nm for the 500 nm period array and at λ = 794 and 860 nm for the 780 nm period array. It can be seen that, for the 500 nm period array at λ = 827 nm, the field is mainly confined around the gold nanoparticle, which is the character of the LSP. In contrast, for the 500 nm period array at λ = 586 nm, the evanescent field above the gold film indicates the excitation of the SPP mode on the interface of the gold film and the SiO_2 spacer. For the 780 nm period array, at both λ = 794 and 860 nm, enhanced near fields in the vicinity of the gold nanoparticle can be seen, but with the addition of an extended evanescent field above the gold film, which is the character of the SPP. These results indicate that the two resonances for strong coupling case carry both the characters of LSPs and SPPs.

The SERS measurements are carried out on a Renishaw confocal Raman microscope with excitation at λ = 783 nm. The Raman signal is collected by a 5× objective (NA = 0.12) and recorded by a thermoelectrically cooled CCD array. To determine the SERS enhancement factor, measurements are made on a 500 μm thick sample cell containing a neat solution of benzenethiol. The SERS enhancement factor is determined from $EF = (I_{SERS}/N_{SERS})/(I_{RF}/N_{RF})$. I_{SERS} and I_{RF} are the intensities of a specific Raman line for the SERS substrate and reference sample, respectively. N_{SERS} and N_{RF} are the numbers of probed molecules in the laser spot for the SERS substrate and reference sample, respectively. The intensity is calculated from the integral of the Raman line of the measured spectrum from which the background has been subtracted and normalized by the laser power and CCD integration time. For N_{SERS}, we assume the benzenethiol surface density is 6.8×10^{14} cm^{-2}.[5] The surface area taken for each gold disk accounts for the top surface as well as the side walls. Therefore, N_{SERS} is calculated as $N_{SERS} = \rho_s S_{gold} A/a^2$, where ρ_s is the benzenethiol surface packing density, S_{gold} is the surface area of one gold disk, a is the period of the array, and A is the laser spot area. N_{RF} is calculated using the molecular weight and volume density of benzenthiol, together with the detection volume. Due to the variation in intensity and collection efficiency with position, the contribution of each molecule in the benzenethiol solution to the measured Raman signal depends on its position. Following the approach of Cai *et al.*,[24] the detection volume is defined as the volume of a hypothetical cylinder for which the intensity and collection efficiency do not vary along the length of the cylinder but only with radial position, where they take values equal to those at the plane of focus in the experiment. The length of the cylinder is chosen so that the total Raman signal resulting from the hypothetical cylinder is equal to that of the experiment.[24] Therefore, the detection volume can be calculated as hA, where h is the effective confocal length, that is, the height of the cylinder. To find the detection volume, we measure the effective confocal length by translating a reference Si sample through the focal volume, and recording the Raman signal at each position.[24−26] For the 5× objective we use, the confocal length is about 2.9 cm, which is much greater than the thickness of the neat benzenethiol sample. Therefore, the thickness of the neat benzenethiol, 500 μm, is used to calculate the detection volume. Therefore, N_{RF} can be calculated from $N_{RF} = N_A \rho h A/M$, where N_A is Avogadro's number, ρ is benzenethiol density, h is the thickness of the neat benzenethiol sample, and M is molar mass of benzenethiol molecules.

The positions of the excitation laser and the Raman Stokes bands 421 and 1074 cm^{-1} of the benzenethiol molecule are shown as dashed lines in Figure 3a. For each periodicity, that is, 350, 500, and 780 nm, different arrays with varying disk diameters are characterized by reflection measurements and SERS measurements. The LSP resonance wavelength changes with the disk diameter. The curves in Figure 3a are spectra of the arrays that give the highest enhancement factor of the 1074 cm^{-1} Raman line for each periodicity. The enhancement of a Raman line depends on the near field enhancement at the wavelengths of both the excitation and the Raman line. For the structure with a period of 780 nm, it can be seen that the wavelengths of the excitation laser and the 1074 cm^{-1} Raman line match the resonance positions closely. For the structures with periods of 350 and 500 nm, it is found that the enhancement factor of the 1074 cm^{-1} Raman line is largest when the LSP resonance wavelength is located between the wavelengths of the excitation and the 1074 cm^{-1} Raman line. This behavior is in agreement with the results of ref 5. The Raman spectra of benzenethiol adsorbed on the three structures are shown in Figure 3b. Figure 3c shows the reflection spectrum and the SERS spectrum of the 780 nm period array as a function of wavelength. The background of the SERS spectrum comes from fluorescence of the SiO_2 layer. It can be seen that the background of the SERS spectrum has a

very similar shape to the reflection spectrum (Figure 3c). The distinctly strong signal around 1100 cm^{-1} corresponds to the position of the lower energy resonance of the 780 nm period array. The intensity of the 421 cm^{-1} Raman line is much larger for the 500 nm period array than the 780 nm period array. For the 780 nm array, the 421 cm^{-1} line is located near a dip in the extinction spectrum, implying that the enhancement of the 421 cm^{-1} Raman line is small for that array. On the other hand, the plasmon resonance for the 500 nm array is close to the 421 cm^{-1} line. The enhancement of the laser excitation is likely to be stronger for the 780 nm array than the 500 nm array due to 780 nm array having a plasmon resonance close to the laser frequency. Nonetheless, the data suggests that the stronger enhancement of the 421 cm^{-1} line for the 500 nm period array leads to a larger overall SERS enhancement. From the data, the EFs of the 1074 cm^{-1} Raman line are found to be 6.5×10^6 for the 350 nm period array, 1.0×10^7 for the 500 nm period array, and 7.2×10^7 for the 780 nm period array. The EFs of the 421 cm^{-1} Raman line are found to be 2.3×10^6 for the 350 nm period array, 1.1×10^7 for the 500 nm period array, and 1.2×10^6 for the 780 nm period array. The strong coupling case (*i.e.*, the 780 period array) provides SERS EF for the 1074 cm^{-1} line that are 7−11 times larger than that of weak coupling cases (350 and 500 nm period arrays), as it offers strong enhancement of the excitation and the Raman scattered signal simultaneously. The total SERS signal of the 1074 cm^{-1} Raman line is higher for the 780 nm period array than that of the 350 and 500 nm period arrays, though the number of the probed molecules on it is smaller for the 780 nm period array due to the smaller density of gold nanoparticles. For comparison, we also fabricate gold disk arrays on a glass substrate and determine the EF of the 1074 cm^{-1} Raman line using the same method. The arrays are arranged as square lattices with periods of 300 or 450 nm. The thicknesses of the gold disks are 40 nm and a variety of samples are fabricated, with disk diameters ranging from 170 to 200 nm. The largest SERS enhancement of the 1074 cm^{-1} Raman line is 3.9×10^5, found on the array with period of 450 nm and disk diameter of 180 nm. The extinction spectrum of this array (not shown) reveals that the LSP resonance is located between the wavelengths of the excitation and the 1074 cm^{-1} Raman line. Compared with the gold nanoparticle array on glass substrate, the double-resonance structure offers SERS EF more than 2 orders of magnitude higher.

We also fabricate silver double-resonance structures. Compared with gold, silver has less loss. Therefore, a higher SERS EF is expected for silver devices. Figure 5 shows the extinction spectrum and SERS spectrum of a structure consisting of a 100 nm thick silver film, a 27 nm thick SiO_2 spacer, and a silver disk array with a period of 780 nm. The silver disks are 147 nm in diameter and 40 nm thick. The extinction spectrum

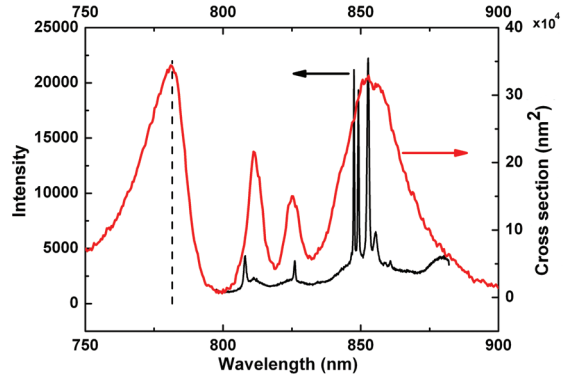

Figure 5. Extinction cross section and SERS spectrum of the silver device.

is taken after the coating of the benzenethiol monolayer. Similar to the gold device, the strong coupling between the LSP on the silver disks and the SPP on the silver film results in the double resonances. The excitation laser is at $\lambda = 782$ nm, which matches with the high energy resonance. The strong enhanced SERS signal around 850 nm corresponds to the low energy resonance. The EFs of the 421and 1074 cm^{-1} Raman lines are found to be 7.7×10^7 and 8.4×10^8, respectively.

In summary, we demonstrate that coupling between LSPs and SPPs enhances the local field intensity and leads to double-resonance features in the extinction spectra of the multiple-layer structure. The SERS enhancement for the double-resonance structure is more than 2 orders of magnitude higher than that of a gold disk array on a glass substrate. The largest SERS enhancement factor is measured to be 7.2×10^7 for gold devices and 8.4×10^8 for silver devices. With the mechanism demonstrated above, the double resonance structure could be optimized further. The near field enhancement of nanoparticles depends on their shape. We anticipate that even larger SERS enhancements will be possible through the use of nanoparticles with other shapes, for example, triangles or rings. Similarly, pairs of particles separated by small gaps could provide a means for improved SERS EF.

Acknowledgment. The authors would like to thank Eric Diebold, Dr. Paul Peng, and Prof. Eric Mazur for use of their Raman confocal microscope. The authors acknowledge support from the Defense Advanced Research Projects Agency (DARPA) and Schlumberger-Doll Research. Fabrication work was carried out at the Harvard Center for Nanoscale Systems, which is supported by the National Science Foundation.

REFERENCES AND NOTES

1. Kneipp, K.; Moskovits, M.; Kneipp, H. Surface-Enhanced Raman Scattering. *Physics and Applications*; Springer: New York, 2007.
2. Kerker, M.; Wang, D.; Chew, H. Surface Enhanced Raman-Scattering (SERS) by Molecules Adsorbed at Spherical Particles. *Appl. Opt.* **1980**, *19*, 4159–4174.
3. Otto, A. The "Chemical" (Electronic) Contribution to Surface-Enhanced Raman Scattering. *J. Raman Spectrosc.* **2005**, *36*, 497–509.

4. Reilly, T. H.; Chang, S.; Corbman, J. D.; Schatz, G. C.; Rowlen, K. L. Quantitative Evaluation of Plasmon Enhanced Raman Scattering from Nanoaperture Arrays. *J. Phys. Chem. C* **2007**, *111*, 1689–1694.
5. McFarland, A. D.; Young, M. A.; Dieringer, J. A.; VanDuyne, R. P. Wavelength-Scanned Surface-Enhanced Raman Excitation Spectroscopy. *J. Phys. Chem. B* **2005**, *109*, 11279–11285.
6. Kahl, M.; Voges, E.; Kostrewa, S.; Viets, C.; Hill, W. Periodically Structured Metallic Substrates for SERS. *Sens. Actuators, B* **1998**, *51*, 285–291.
7. Schmidt, J. P.; Cross, S. E.; Buratto, S. K. Surface-Enhanced Raman Scattering from Ordered Ag Nanocluster Arrays. *J. Chem. Phys.* **2004**, *121*, 10657–10659.
8. Su, K. H.; Wei, Q. H.; Zhang, X. Tunable and Augmented Plasmon Resonances of Au/SiO_2/Au Nanodisks. *Appl. Phys. Lett.* **2006**, *88*, 063118.
9. Felidj, N.; Lau Truong, S.; Aubard, J.; Levi, G.; Krenn, J. R.; Hohenau, A.; Leitner, A.; Aussenegg, F. R. Gold Particle Interaction in Regular Arrays Probed by Surface Enhanced Raman Scattering. *J. Chem. Phys.* **2004**, *120*, 7141–7146.
10. Banaee, M. G.; Crozier, K. B. Gold Nanorings as Substrates for Surface-Enhanced Raman Scattering. *Opt. Lett.* **2010**, *35*, 760–762.
11. Maier, S. A. *Plasmonics: Fundamentals and Applications*; Springer: New York, 2007.
12. Kelly, K. L.; Coronado, E.; Zhao, L. L.; Schatz, G. C. The Optical Properties of Metal Nanoparticles: The Influence of Size, Shape, and Dielectric Environment. *J. Phys. Chem. B* **2003**, *107*, 668–677.
13. Oldenburg, S. J.; Westcott, S. L.; Averitt, R. D.; Halas, N. J. Surface Enhanced Raman Scattering in the Near Infrared Using Metal Nanoshell Substrates. *J. Chem. Phys.* **1999**, *111*, 4729–4735.
14. Aizpurua, J.; Hanarp, P.; Sutherland, D. S.; Kall, M.; Bryant, G. W.; Garcia de Abajo, F. J. Optical Properties of Gold Nanorings. *Phys. Rev. Lett.* **2003**, *90*, 057401.
15. Grand, J.; Lamy de la Chapelle, M.; Bijeon, J.-L.; Adam, P.-M.; Vial, A.; Royer, P. Role of Localized Surface Plasmons in Surface-Enhanced Raman Scattering of Shape-Controlled Metallic Particles in Regular Arrays. *Phys. Rev. B* **2005**, *72*, 033407.
16. Zou, S.; Schatz, G. C. Silver Nanoparticle Array Structures that Produce Giant Enhancement in Electromagnetic Fields. *Chem. Phys. Lett.* **2005**, *403*, 62–67.
17. Chu, Y.; Schonbrun, E.; Yang, T.; Crozier, K. B. Experimental Observation of Narrow Surface Plasmon Resonances in Gold Nanoparticle Arrays. *Appl. Phys. Lett.* **2008**, *93*, 181108.
18. Gantzounis, G.; Stefanou, N.; Papanikolaou, N. Optical Properties of Periodic Structures of Metallic Nanodisks. *Phys. Rev. B* **2008**, *77*, 035101.
19. Stuart, H. R.; Hall, D. G. Enhanced Dipole−Dipole Interaction between Elementary Radiators near a Surface. *Phys. Rev. Lett.* **1998**, *80*, 5663–5666.
20. Papanikolaou, N. Optical Properties of Metallic Nanoparticle Arrays on a Thin Metallic Film. *Phys. Rev. B* **2007**, 235426.
21. Kinnan, M. K.; Chumanov, G. Surface Enhanced Raman Scattering from Silver Nanoparticle Arrays on Silver Mirror Films: Plasmon-Induced Electronic Coupling as the Enhancement Mechanism. *J. Phys. Chem. C* **2007**, *111*, 1801018017.
22. Chu, Y.; Crozier, K. B. Experimental Study of the Interaction between Localized and Propagating Surface Plasmons. *Opt. Lett.* **2009**, *34*, 244–246.
23. Ghoshal, A.; Divliansky, I.; Kik, P. G. Experimental Observation of Mode-Selective Anticrossing in Surface-Plasmon-Coupled Metal Nanoparticle Arrays. *Appl. Phys. Lett.* **2009**, *94*, 171108.
24. Cai, W. B.; Ren, B.; Li, X. Q.; She, C. X.; Liu, F. M.; Cai, X. W.; Tian, Z. Q. Investigation of Surface-Enhanced Raman Scattering from Platinum Electrodes Using a Confocal Raman Microscope: Dependence of Surface Roughening Pretreatment. *Surf. Sci.* **1998**, *406*, 9–22.
25. LeRu, E. C.; Blackie, E.; Meyer, M.; Etchegoin, P. G. Surface Enhanced Raman Scattering Enhancement Factors: a Comprehensive Study. *J. Phys. Chem. C* **2007**, *111*, 13794–13803.
26. Haynes, C. L.; VanDuyne, R. P. Plasmon- Sampled Surface-Enhanced Raman Excitation Spectroscopy. *J. Phys. Chem. B* **2003**, *107*, 7426–7433.